Improving Neural Network-based Multidimensional Projections

Mateus Espadoto[1][a], Nina S. T. Hirata[1][b], Alexandre X. Falcão[2][c] and Alexandru C. Telea [3][d]
[1]*Institute of Mathematics and Statistics, University of São Paulo, São Paulo, Brazil*
[2]*Institute of Computing, University of Campinas, Campinas, Brazil*
[3]*Department of Information and Computing Sciences, Utrecht University, Utrecht, The Netherlands*
{*mespadot, nina*}*@ime.usp.br, afalcao@ic.unicamp.br, a.c.telea@uu.nl*

Keywords: Dimensionality Reduction, Machine Learning, Neural Networks, Multidimensional Projections.

Abstract: Dimensionality reduction methods are often used to explore multidimensional data in data science and information visualization. Techniques of the SNE-class, such as t-SNE, have become the standard for data exploration due to their good visual cluster separation, but are computationally expensive and don't have out-of-sample capability by default. Recently, a neural network-based technique was proposed, which adds out-of-sample capability to t-SNE with good results, but with the disavantage of introducing some diffusion of the points in the result. In this paper we evaluate many neural network-tuning strategies to improve the results of this technique. We show that a careful selection of network architecture, loss function and data augmentation strategy can improve results.

1 INTRODUCTION

Exploration of high-dimensional data is a key task in statistics, data science, and machine learning. This task can be very hard, due to the large size of such data, both in the number of samples and in number of variables recorded per observation (also called dimensions or features). As such, high-dimensional data visualization has become an important field in information visualization (infovis) (Kehrer and Hauser, 2013; Liu et al., 2015).

Dimensionality reduction (DR) methods, also called projections, play an important role in the above problem. Compared to all other high-dimensional visualization techniques, they scale much better in terms of both the number of samples and the number of dimensions they can show on a given screen space area. As such, DR methods have become the tool of choice for exploring data which have an especially high number of dimensions (tens up to hundreds) and/or in applications where the identity of dimensions is less important. Over the years, many DR techniques have been proposed (van der Maaten and Postma, 2009; Nonato and Aupetit, 2018), using several different approaches and achieving varying degrees of success.

Currently, t-SNE (van der Maaten and Hinton, 2008) is one of the most known and used DR technique, due to the visually appealing projections it creates, with good visual segregation of clusters of similar observations. However, t-SNE comes with some downsides: It is slow to run on datasets of thousands of observations or more, due to its quadratic time complexity; its hyperparameters can be hard to tune to get a good result (Wattenberg, 2016); its results are very sensitive to data changes, *e.g.*, adding more samples may result in a completely different projection; and it cannot project out-of-sample data, which is useful for time-dependent data analysis (Rauber et al., 2016; Nonato and Aupetit, 2018).

A recent work (Espadoto et al., 2019) tried to address the above issues by using deep learning: A fully-connected *regression* neural network trained from a small subset of samples of a high-dimensional dataset and their corresponding 2D projection (produced by any DR technique). Next, the network can infer the 2D projection on any high-dimensional dataset drawn from a similar distribution as the training set. The authors claim several advantages to this: The network infers much faster than the underlying DR technique (orders of magnitude faster than t-SNE, for example), and works deterministically, thereby providing out-of-sample capability by construction.

[a] https://orcid.org/0000-0002-1922-4309
[b] https://orcid.org/0000-0001-9722-5764
[c] https://orcid.org/0000-0002-2914-5380
[d] https://orcid.org/0000-0003-0750-0502

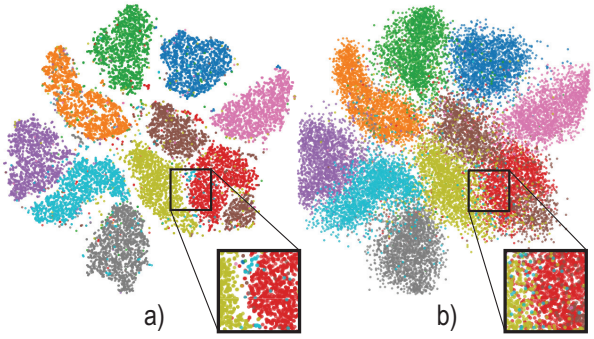

Figure 1: Example of diffusion introduced by the NN projection. (a) Ground-truth t-SNE projection (b) Inferred NN projection (10K samples). Insets show diffusion details.

However, this approach (further called Neural Network (NN) projection for brevity) has two limitations. First, and most seriously, the authors do not show that learning occurs *robustly*, *i.e.*, that the presented results are not singular cases due to lucky settings of the many NN hyperparameters such as loss function used, optimizer, regularization, or training-set size. Deep learning is notoriously sensitive to such settings, so fully exploring the NN hyperparameter space is needed before one can make strong assertions about the learning quality (Feurer and Hutter, 2019; Ilievski et al., 2017). This is especially important for the DR approach in (Espadoto et al., 2019) since, if this approach were *indeed* robust, it would represent a major improvement to DR state-of-the-art, given its simplicity, genericity, and speed. Secondly, it is visible from (Espadoto et al., 2019) that the NN projections have some amount of *diffusion*, *i.e.*, they separate similar-sample clusters less clearly than in a ground-truth t-SNE projection (see *e.g.* Figure 1). While visually salient, it is unclear how much this diffusion affects the quality of a projection; and how much this diffusion depends on hyperparameter settings. Diffusion can have several causes, *e.g.*: (1) underfitting, by training for too few epochs or having too little data to learn from; (2) overfitting, by not having proper regularization or also by having too little data to learn from; (3) imperfect optimization, with the optimizer getting stuck in local minima. However, which is the precise cause of diffusion is still unknown and, thus, not controllable.

In this paper, we aim to answer both above issues with the following contributions:

- we quantify the NN projection *quality* by using four well-known projection quality metrics;
- we explore the *hyperparameter space* of NN projections, showing how these influence the results' quality, gauged by the projection quality metrics;
- we show that NN projections are *stable* with respect to hyperparameter settings, thereby completing the claim made by (Espadoto et al., 2019) that they can be reliably used for out-of-sample and noisy-data contexts.

The structure of this paper is as follows. Section 2 discusses related work on DR and neural networks. Section 3 details our experimental setup. Section 4 presents our results, which are next discussed in Section 5. Section 6 concludes the paper.

2 RELATED WORK

Related work can be split into dimensionality reduction and deep learning, as follows.

Dimensionality reduction: Let $\mathbf{x} = (x^1, \ldots, x^n)$, $x^i \in \mathbb{R}, 1 \leq i \leq n$ be an n-dimensional (nD) real-valued sample, and let $D = \{\mathbf{x}_i\}$, $1 \leq i \leq N$ be a dataset of N samples. Thus, D can be seen as a table with N rows (samples) and n columns (dimensions). A projection technique is a function $P : \mathbb{R}^n \rightarrow \mathbb{R}^q$ where $q \ll n$, and typically $q = 2$. The projection $P(\mathbf{x})$ of a sample $\mathbf{x} \in D$ is a 2D point. Projecting a set D yields thus a 2D scatterplot, which we denote next as $P(D) = \{P(\mathbf{x}) | \mathbf{x} \in D\}$.

Many Dimensionality Reduction (DR) techniques have been developed over the years, with different trade-offs of ease of use, scalability, distance preservation, and out-of-sample capability. One of the most widely used DR method is Principal Component Analysis (Peason, 1901; Jolliffe, 1986) (PCA), due to its ease of use and scalability. Manifold Learners, such as MDS (Torgerson, 1958), Isomap (Tenenbaum et al., 2000) and LLE (Roweis and Saul, 2000) try to reproduce in 2D the high-dimensional manifold on which data is embedded, with the goal of capturing nonlinear data structures. More recently, UMAP (Uniform Manifold Approximation and Projection) (McInnes and Healy, 2018) was proposed, based on simplicial complexes and manifold learning techniques.

The SNE (Stochastic Neighborhood Embedding) class of techniques, with t-SNE (van der Maaten and Hinton, 2008) being its most successful member, models similarity between samples as a probability distribution of two points being neighbors of each other, and try to reproduce the same probabilities in 2D. As outlined in Section 1, a key feature of t-SNE is its ability to separate sample clusters very well in visual space, which is very helpful for unsupervised learning scenarios.

Deep learning: Building well-performing neural network (NN) architectures is very challenging due

to the many degrees of freedom allowed by their design process. We outline below five typical such degrees of freedom.

Network Architecture: Part of the power of NNs comes from having many possible architectures, in particular regarding number of layers and layer size, if we restrict ourselves to fully-connected networks. There is not a one-size-fits-all set of guidelines to architecting NNs, which are typically created empirically.

Regularization: NNs can be prone to overfitting, which makes them fail to generalize during inference for unseen data. Regularization techniques try to address this by making the learning process harder, so the NN can train for more epochs and generalize better. Regularization techniques include L_2, L_1, max-norm, early stopping, and data augmentation. The L_k regularization techniques, also known as *weight pruning* ($k = 1$) and *weight decay* ($k = 2$), work by adding a penalization term of the form $\lambda \|\boldsymbol{w}\|^k$ to the NN loss function, which equals the k-norm of the weights $\boldsymbol{w}$ of a selected network layer. The parameter λ controls the amount of regularization.

L_1 (Park and Hastie, 2007) regularization decreases layer weights with the less important getting down to zero, leading to models with sparse weights. L_2 (Krogh and Hertz, 1992) regularization decreases layer weights to small but non-null values, leading to models where every weight only slightly contributes to the model. Both regularization techniques were observed to help prevent overfitting. Max-norm (Srebro and Shraibman, 2005), originally proposed for Collaborative Filtering, was successfully applied as a regularizer for NNs. It imposes a maximum value γ for the norm of the layer weights. This way, weight values are kept under control, similarly to L_2, but using a hard limit. Early stopping (Yao et al., 2007) is a simple but effective way to prevent overfitting, especially when combined with the other regularization techniques outlined above. The idea is to stop training when the training loss J_T and validation losses J_V diverge, *i.e.*, J_T keeps decreasing while J_V stops decreasing or worse, starts increasing, both of which signal overfitting.

Optimizers: Different optimizers are used for minimizing the non-linear NN cost. The most used optimizers are based on Mini-batch Stochastic Gradient Descent (SGD) which is a variant of classic Gradient Descent (GD). GD aims to find optimal weights $\boldsymbol{w}$ (that minimize the error created by the NN for the training set) by adjusting these iteratively via the gradient ∇J of the loss function J with respect to $\boldsymbol{w}$ as

$$\boldsymbol{w}_t = \boldsymbol{w}_{t-1} - \eta \nabla J \tag{1}$$

where the learning rate η controls how large is each update step t. Classic GD uses all data samples at each iteration of Equation 1, which is costly for large datasets. Stochastic Gradient Descent (SGD) alleviates this by using only one sample, picked randomly, at each iteration. This speeds up computation at the cost of having to solve a harder problem, as there is less information available to the optimizer. A commonly used optimizer today is Mini-batch SGD, which uses one batch of samples for each GD iteration, thus achieves a compromise between classic GD and SGD. The Momentum method (Qian, 1999) improves SGD convergence by adding to the update vector $\mathbf{u}_t = \eta \nabla J$ at step t a fraction ν of the previous update vector $\mathbf{u}_{t-1}$ (Equation 2), *i.e.*

$$\boldsymbol{w}^t = \boldsymbol{w}_{t-1} - (\nu \mathbf{u}_{t-1} + \mathbf{u}_t) \tag{2}$$

However, tuning the learning rate η is not trivial: Too small values may make the NN take too long to converge; conversely, too high values may make training miss good minima. Adaptive learning optimizers, such as Adaptive Moment Estimation (ADAM) (Kingma and Ba, 2014), alleviate this by using squared gradients to compute the learning rate dynamically. This greatly improves convergence speed. However, (Wilson et al., 2017) found that ADAM can find solutions that are worse than those found by Mini-batch SGD. Solving this problem is still an open research question.

Data augmentation: Such techniques generate data that are similar, but not identical, to existing training data, to improve training when training-sets are small. Such techniques highly depend on the data type. Augmentation can be used for regularization since adding more training data creates models that generalize better.

Loss functions: Finally, one needs to select an appropriate loss function J. For regression problems, commonly used loss functions are Mean Squared Error (MSE), Mean Absolute Error (MAE), logcosh, and Huber loss. Table 1 shows the definitions of these functions, where $\hat{\mathbf{y}} = \{\hat{y}_i\}$ is the inferred output vector of the NN and $\mathbf{y} = \{y_i\}$ is the training sample $\hat{\mathbf{y}}$ should match. MSE and logcosh are smoother functions which are easier to optimize by GD or similar methods outlined above. MAE is harder to optimize since its gradient is constant. The Huber loss is somewhere in between the above, according to the parameter α: For values of α near zero, Huber behaves like MAE; for larger α values, it behaves like MSE. MAE

and Huber losses are known to be more robust to outliers than MSE.

Table 1: Typical NN loss functions.

Function	Definition
MSE	$\frac{1}{n}\sum_{i=1}^{n}(y_i-\hat{y}_i)^2$
MAE	$\frac{1}{n}\sum_{i=1}^{n}\lvert y_i-\hat{y}_i\rvert$
logcosh	$\frac{1}{n}\sum_{i=1}^{n} log(cosh(y_i-\hat{y}_i))$
Huber	$\begin{cases}\frac{1}{2}(y-\hat{y})^2 & \text{if} \lvert y-\hat{y}\rvert \leq \alpha \\ \alpha\lvert y-\hat{y}\rvert-\frac{1}{2}\alpha & \text{otherwise}\end{cases}$

Deep learning projections: The method proposed in (Espadoto et al., 2019) uses deep learning to construct projections as follows. Given a dataset $D \subset \mathbb{R}^n$, a training subset $D_t \subset D$ thereof is selected, and projected by a user-selected method (t-SNE or any other) to yield a so-called training projection $P(D_t) \subset \mathbb{R}^2$. Next, D_t is fed into a three-layer, fully-connected, regression neural network which is trained to output a 2D scatterplot $NN(D_t) \subset \mathbb{R}^2$ by minimizing the mean squared error between $P(D_t)$ and $NN(D_t)$. After that, the network is used to construct projections of unseen data by means of 2-dimensional, non-linear regression. Note that this approach is fundamentally different from *autoencoders* (Hinton and Salakhutdinov, 2006) which do not learn from a training projection P, but simply aim to extract, in an unsupervised way, latent low-dimensional features that best represent the input data. The NN projection method is simple to implement, generically learns any projection P for any dataset $D \subset \mathbb{R}^n$, and is orders of magnitudes faster than classical projection techniques, in particular t-SNE. However, as outlined in Section 1, the quality and stability of this method *vs* parameter setting has not yet been assessed in detail. The goal of this paper is to correct this important weakness of the work in (Espadoto et al., 2019).

3 METHOD

3.1 Parameter space exploration

To achieve our objectives, listed in Section 1, we designed and executed a set of experiments, detailed next. For each experiment, we train and test the NN projection with various combinations of datasets and hyperparameter settings, and then interpret the obtained results both quantitatively and qualitatively. All parameter values used for each experiment are detailed in this section. Early stopping was used on all experiments, stopping training if the validation loss stops decreasing for more than 10 epochs, and except for the experiment with different optimizers, ADAM was used on all experiments as well. As dataset, we use MNIST (LeCun et al., 2010), which contains 70K samples of handwritten digits from 0 to 9, rendered as 28x28-pixel grayscale images, flattened to 784-element vectors, with 10K test-set samples, and varying training-set sizes of 2K, 5K, 10K and 20K samples. We chose this dataset as it is complex, high-dimensional, has a clear class separation, and it is well known in dimensionality reduction literature. MNIST was also used in (Espadoto et al., 2019), which makes it easy to compare our results.

In line with the design choices available to NNs outlined in Section 2, we explore the performance of NN projections in the following directions.

Network Architecture (Section 4.5): We selected three sizes of neural networks with 360 (small), 720 (medium) and 1440 (large) total number of units, and distributed them into three different layouts, namely straight (st), wide (wd) and bottleneck (bt), thus yielding nine different architectures, as follows:

- *Small - straight*: 120, 120 and 120 units;
- *Small - wide*: 90, 180 and 90 units;
- *Small - bottleneck*: 150, 60 and 150 units;
- *Medium - straight*: 240, 240 and 240 units;
- *Medium - wide*: 180, 360 and 180 units;
- *Medium - bottleneck*: 300, 120 and 300 units;
- *Large - straight*: 480, 480 and 480 units;
- *Large - wide*: 360, 720 and 360 units;
- *Large - bottleneck*: 600, 240 and 600 units.

Besides these, we also tested the architecture in (Espadoto et al., 2019), called next *Standard*, which has three fully-connected hidden layers, with 256, 512, and 256 units respectively. All architectures use ReLU activation functions, followed by a 2-element layer which uses the sigmoid activation function to encode the 2D projection.

Regularization (Section 4.1): We explored the following regularization techniques:

- L_1 with $\lambda \in \{0, 0.001, 0.01, 0.1\}$ with 0 meaning no regularization;
- L_2 with $\lambda \in \{0, 0.001, 0.01, 0.1\}$ with 0 meaning no regularization;
- Max-norm constraint, with $\gamma \in \{0, 1, 2, 3\}$, with 0 meaning no constraint;

Optimizers (Section 4.2): We studied two optimizers: ADAM and Mini-batch SGD with learning rates $\eta \in \{0.01, 0.001\}$ and $\nu = 0.9$. In both cases, we set

the batch size at 32 samples.

Data augmentation (Section 4.3): We explored two data augmentation strategies:

- *Noise Before:* We add Gaussian noise of zero mean and different standard deviations $\sigma \in \{0, 0.001, 0.01\}$, with 0 meaning no noise, to the high-dimensional training data, project this entire (noise + clean samples) dataset, and ask the NN to learn the projection. The idea is that, if the projection to learn (t-SNE in our case) can successfully create well-separated clusters even for noisy data, then our NN should learn how to do this as well;
- *Noise After:* We create the training projection from clean data. We next add Gaussian noise (same σ as before) to the data and train the NN to project the entire (noise + clean samples) dataset to the clean projection. The aim is to force the NN to learn to project slightly different samples to the same 2D point.

Loss functions (Section 4.4): We studied four types of loss functions: Huber, with parameters $\alpha \in \{1, 5, 10, 20, 30\}$; Mean Squared Error (MSE), used by (Espadoto et al., 2019); Mean Absolute Error (MAE); and logcosh.

Adding more data: For all above directions, we use different training-set sizes (2K, 5K, 10K and 20K samples) to evaluate how this affects the results – that is, how the NN projection quality depends on *both* hyperparameter values and training-set size.

3.2 Quality metrics

To evaluate the quality of the obtained projections, we used the following four metrics well-known in the DR literature (see Table 2). Of these, note that the original paper (Espadoto et al., 2019) only discusses Neighborhood Hit.

Trustworthiness T: Measures the fraction of points in D that are also close in $P(D)$ (Venna and Kaski, 2006). T tells how much one can trust that local patterns in a projection, *e.g.* clusters, show actual patterns in the data. $U_i^{(K)}$ is the set of points that are among the K nearest neighbors of point i in the 2D space but not among the K nearest neighbors of point i in $\mathbb{R}^n$; and $r(i, j)$ is the rank of the 2D point j in the ordered set of nearest neighbors of i in 2D. We chose $K = 7$ for this study, following (van der Maaten and Postma, 2009; Martins et al., 2015);

Continuity C: Measures the fraction of points in $P(D)$ that are also close in D (Venna and Kaski, 2006). $V_i^{(K)}$ is the set of points that are among the K nearest neighbors of point i in $\mathbb{R}^n$ but not among the K nearest neighbors in 2D; and $\hat{r}(i, j)$ is the rank of the $\mathbb{R}^n$ point j in the ordered set of nearest neighbors of i in $\mathbb{R}^n$. As in the case of T, we chose $K = 7$;

Neighborhood Hit NH: Measures how well-separable labeled data is in a projection $P(D)$ from perfect separation ($NH = 1$) to no separation ($NH = 0$) (Paulovich et al., 2008). NH equals the number $\mathbf{y}_K^l$ of the K nearest neighbors of a point $\mathbf{y} \in P(D)$, denoted by $\mathbf{y}_K$, that have the same label as $\mathbf{y}$, averaged over $P(D)$. In this paper, we used $K = 7$;

Shepard diagram correlation R: Shepard diagrams are scatterplots of pairwise (Euclidean) distances between all points in $P(D)$ *vs* corresponding distances in D (Joia et al., 2011). Plots close to the main diagonal indicate better overall distance preservation. Plot areas below, respectively above, the diagonal indicate distance *ranges* for which false and missing neighbors, respectively, occur. We measure the quality of a Shepard diagram by computing its Spearman ρ rank correlation. A value of $R = 1$ indicates a perfect (positive) correlation of distances.

Table 2: Quality metrics. Right column gives metric ranges, with optimal values in bold.

Metric	Definition
T	$1 - \frac{2}{NK(2n-3K-1)} \sum_{i=1}^{N} \sum_{j \in U_i^{(K)}} (r(i,j) - K)$
C	$1 - \frac{2}{NK(2n-3K-1)} \sum_{i=1}^{N} \sum_{j \in V_i^{(K)}} (\hat{r}(i,j) - K)$
NH	$\frac{1}{N} \sum_{\mathbf{y} \in P(D)} \frac{\mathbf{y}_k^l}{\mathbf{y}_k}$
R	$\rho(\lVert \mathbf{x}_i - \mathbf{x}_j \rVert, \lVert P(\mathbf{x}_i) - P(\mathbf{x}_j) \rVert), 1 \leq i \leq N, i \neq j$

4 RESULTS

We next present the details of each experiment along with the obtained results.

4.1 Regularization

We use increasing amounts of L_1 and L_2 regularization to test if, by having a penalty term on the cost function during training, the NN can generalize better. We use L_1 and L_2 separately, to study how their effects compare to each other.

Figures 2 and 3 show the results. We see that, for both L_1 and L_2, the higher the regularization values λ, the worse are the results. For instance, the resulting projection (train or test) becomes completely unrelated to the ground truth (training t-SNE projection) when $\lambda = 0.1$. Separately, we see that L_2 regularization performs better – that is, it produces projections

Table 3: Effect of **regularization**. Rows show metrics for t-SNE (*GT* row) *vs* NN projections using different training-set sizes. Bold shows values closest to *GT*.

a) L_1 **regularization**

Model	λ	*NH*	*T*	*C*	*R*	# epochs	Time (s)
GT		0.929	0.990	0.976	0.277		
2K	0	**0.705**	**0.843**	**0.957**	**0.443**	50	6.20
	0.001	0.677	0.827	0.948	0.439	58	7.14
	0.01	0.660	0.815	0.945	0.438	94	10.93
	0.1	0.632	0.806	0.943	0.454	82	9.98
5K	0	**0.738**	**0.871**	**0.962**	**0.423**	26	7.22
	0.001	0.692	0.845	0.953	0.436	38	10.05
	0.01	0.670	0.835	0.947	0.427	68	18.29
	0.1	0.599	0.815	0.945	0.459	53	14.58
10K	0	**0.834**	**0.902**	**0.968**	**0.337**	45	22.32
	0.001	0.753	0.852	0.958	0.348	31	16.09
	0.01	0.722	0.833	0.951	0.352	39	19.12
	0.1	0.665	0.811	0.947	0.345	61	30.67
20K	0	**0.885**	**0.922**	**0.967**	**0.341**	49	47.28
	0.001	0.816	0.883	0.960	0.364	30	29.35
	0.01	0.743	0.842	0.954	0.366	28	26.89
	0.1	0.707	0.822	0.946	0.364	25	24.17

b) L_2 **regularization**

NH	*T*	*C*	*R*	# epochs	Time (s)
0.929	0.990	0.976	0.277		
0.695	0.839	0.956	0.437	35	4.61
0.711	**0.847**	**0.958**	0.432	29	4.27
0.684	0.834	0.954	0.433	42	5.57
0.683	0.830	0.952	**0.428**	68	8.54
0.767	**0.880**	**0.963**	0.422	53	14.33
0.742	0.875	**0.963**	0.419	28	7.71
0.733	0.866	0.959	**0.416**	55	15.24
0.709	0.860	0.958	0.429	45	12.51
0.833	**0.899**	**0.967**	0.342	43	20.93
0.821	**0.899**	0.966	0.340	55	27.88
0.798	0.880	0.963	0.337	34	17.37
0.773	0.865	0.961	**0.336**	36	18.48
0.885	**0.922**	**0.967**	0.341	46	43.49
0.870	0.915	0.966	0.343	34	33.06
0.853	0.902	0.963	0.344	40	38.05
0.826	0.883	0.960	**0.339**	38	37.87

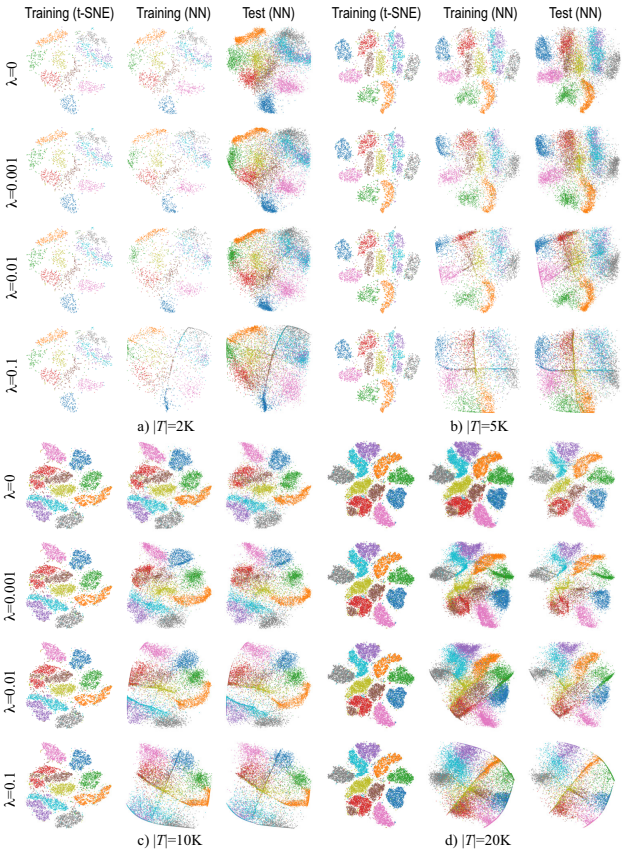

Figure 2: L_1 **regularization:** Effect of λ for different training-set sizes. Compare the ground truth (training-set, projected by t-SNE) with the NN results on the training-set, respectively test-set.

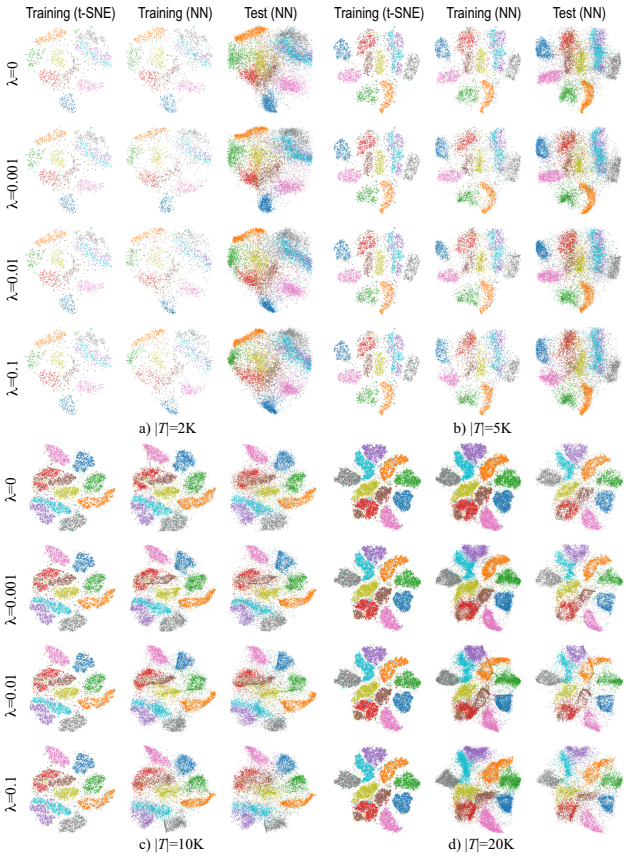

Figure 3: L_2 **regularization:** Effect of λ for different training-set sizes. Compare the ground truth (training-set, projected by t-SNE) with the NN results on the training-set, respectively test-set.

which are closer to the ground truth than the corresponding projections produced using L_1 regularization for the same λ values. Table 3 confirms the above visual findings by showing quality metrics for the L_1 and L_2 regularization experiments. Overall, we see that L_2 regularization produces *NH*, *T*, and *C* metrics closer to the ground-truth (GT) values than L_1 regularization. This table also shows another interesting insight: The NN projections yield *higher* Shepard correlation *R* values than the ground truth t-SNE projection, for all regularization settings (slightly higher for L_1 than L_2). This tells us that the NN aims to preserve the *n*D distances in the 2D projection *more* than the t-SNE projection does (see definition of *R*,

Table 2). This explains, in turn, the diffusion we see in the NN projections. In contrast, t-SNE does not aim to optimize for distance preservation, but neighborhood preservation, which results in a better cluster separation but lower R values.

The rightmost two columns in Tables 3(a,b) show the training effort needed for convergence (epochs and seconds). We see that convergence is achieved *for all cases* in under 70 epochs, regardless of the regularization type (L_1 or L_2) or strength λ. Also, L_1 and L_2 regularization have comparable costs, with L_2 being slightly faster than L_1 for smaller training datasets. Overall, the above tells us that the NN converges robustly regardless of regularization settings.

Table 4: Effect of **max-norm**. Metrics shown for t-SNE (*GT* row) *vs* NN projections using different training-set sizes. Bold shows values closest to *GT*.

Model	γ	*NH*	*T*	*C*	*R*	# epochs	Time (s)
GT		0.929	0.990	0.976	0.277		
2K	0	**0.701**	0.839	0.956	0.443	44	5.45
	1	0.692	0.836	0.956	**0.431**	32	4.47
	2	0.699	**0.842**	**0.957**	0.441	45	5.80
	3	0.698	0.837	0.956	0.441	31	4.47
5K	0	**0.759**	**0.881**	**0.964**	**0.417**	51	13.34
	1	0.756	0.880	**0.964**	0.421	40	10.70
	2	0.740	0.866	0.961	0.420	24	7.05
	3	0.755	0.879	0.963	0.423	48	13.23
10K	0	0.824	0.898	0.966	**0.337**	37	18.14
	1	**0.840**	0.904	0.967	0.338	31	15.43
	2	0.829	0.903	0.967	0.340	37	18.67
	3	0.837	**0.905**	**0.968**	0.338	53	26.63
20K	0	**0.886**	**0.923**	**0.967**	0.342	56	52.65
	1	0.870	0.918	0.967	**0.340**	26	25.22
	2	0.881	0.917	0.967	0.341	30	28.88
	3	0.879	0.920	0.967	0.345	34	34.11

Next, we study max-norm regularization, to see how this affects the NN generalization capability. Figure 4 shows that the projection quality is not strongly dependent on γ, and the metrics in Table 4 confirm this. More importantly, we see that max-norm yields projections which are better in terms of all quality metrics than L_1 and L_2 regularization, and closer to the t-SNE ground truth. Effort-wise, max-norm regularization is very similar to L_1 and L_2 (compare rightmost columns in Table 4 with those in Table 3(a,b)). In conclusion, for this particular problem we determine that regularization brings no clear benefit.

4.2 Optimizer

The quality of the NN projection obviously depends on how well the optimization method used during training can minimize the cost function (Section 2). To find out how the projection quality is influenced by optimization choices, we trained the NN using the ADAM optimizer with its default settings, and also with SGD with learning rates $\eta \in \{0.01, 0.001\}$. Figure 5 shows that the ADAM optimizer produces results with considerably less diffusion than SGD. Table 5 clearly confirms this, as ADAM scores better than SGD for all considered quality metrics. We also see here that ADAM converges much faster than SGD. Since, additionally, ADAM works well with its default parameters, we conclude that this is the optimizer of choice for our problem.

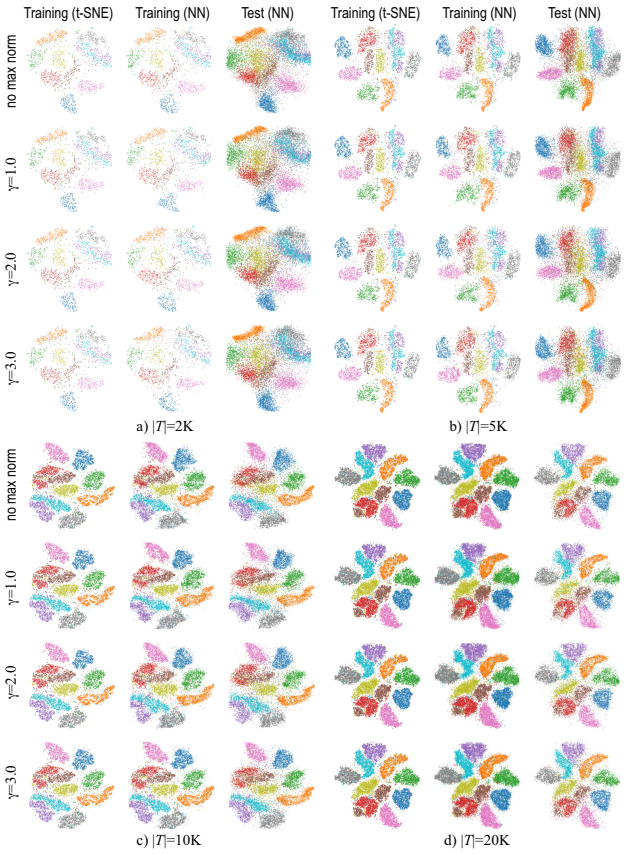

Figure 4: **Max-norm:** Effect of γ for different training-set sizes. Compare the ground truth (training-set, projected by t-SNE) with the NN results on the training-set, respectively test-set.

Table 5: Effect of **optimizers**. Metrics shown for t-SNE (*GT* row) *vs* NN projections using different training-set sizes. Bold shows values closest to *GT*.

Model	Optimizer (η)	*NH*	*T*	*C*	*R*	# epochs	Time (s)
GT		0.929	0.990	0.976	0.277		
2K	ADAM	**0.696**	**0.841**	**0.956**	**0.447**	30	3.72
	SGD (0.01)	0.625	0.791	0.938	0.464	97	8.32
	SGD (0.001)	0.610	0.787	0.938	0.464	455	36.56
5K	ADAM	**0.733**	**0.861**	**0.960**	**0.421**	19	5.27
	SGD (0.01)	0.655	0.817	0.945	0.439	86	16.90
	SGD (0.001)	0.641	0.808	0.942	0.443	402	77.17
10K	ADAM	**0.842**	**0.905**	**0.968**	**0.343**	56	26.51
	SGD (0.01)	0.707	0.821	0.949	0.362	75	28.55
	SGD (0.001)	0.690	0.812	0.948	0.360	392	147.60
20K	ADAM	**0.882**	**0.920**	**0.968**	**0.339**	43	40.77
	SGD (0.01)	0.769	0.838	0.952	0.356	129	94.30
	SGD (0.001)	0.754	0.836	0.952	0.370	423	309.19

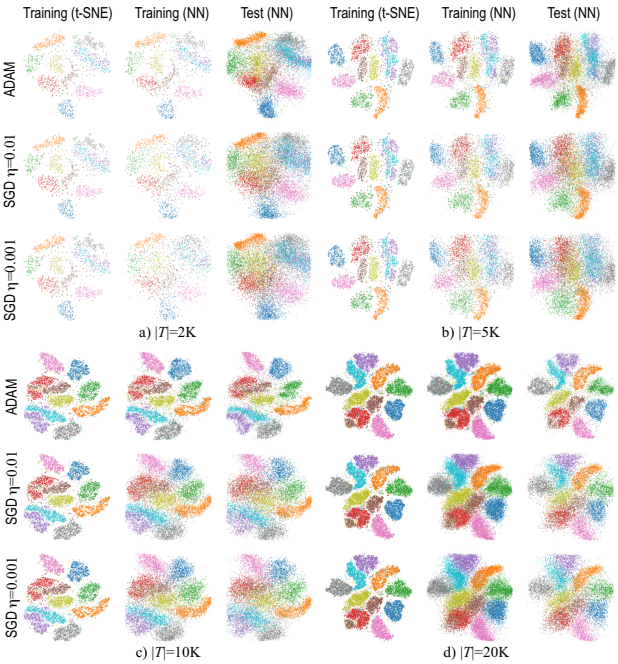

Figure 5: **Optimizer:** Effects of different settings (ADAM, SGD with $\eta \in \{0.001, 0.01\}$) for different training-set sizes. Compare the ground truth (training-set, projected by t-SNE) with the NN results on the training-set, respectively test-set.

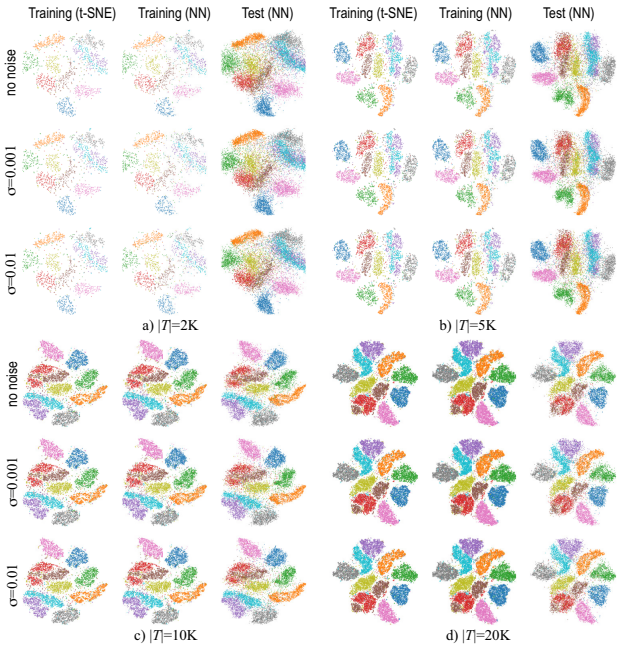

Figure 6: **Noise after** data augmentation: Effect of noise strength $\sigma \in \{0, 0.001, 0.01\}$. Compare the ground truth (training-set, projected by t-SNE) with the NN results on the training-set, respectively test-set.

4.3 Noise-based data augmentation

Here we turn to data augmentation to try to address the problem of reducing diffusion in the NN projection. For this, we add noise to the data as described in Section 3.1 to observe if it improves learning. Figures 6 and 7 show that both the *Noise before* and *Noise after* strategies produce quite similar results, which are also close to the ground truth. Table 7(a,b) confirms this, additionally showing that the *Noise after* strategy yields slightly higher quality metrics on average than *Noise before*. More importantly, if we compare these values with those obtained by trying different regularization techniques and optimizers (Tables 3-4), we see that *Noise after* slightly improves the projection quality.

4.4 Loss function

Next we study the effect of using different loss functions. Figure 8 shows that MAE produces visual clusters that are slightly sharper than the ones created with the other loss functions studied. Also, we see that this effect is more pronounced on tests with lower numbers of training samples. This effect is confirmed by looking at the quality metrics in Table 6: For instance, using MAE yields an increase of *NH* from roughly 0.70 (when using the other loss functions) to roughly 0.74 for the smallest test-set of 2K samples; for the largest test-set of 20K samples, the comparable *NH* increase is from roughly 0.87 to 0.88. Still, MAE

Table 6: Effect of different **loss functions**. Rows show metrics for t-SNE (*GT* row) *vs* NN projections using different training-set sizes. Bold shows values closest to *GT*.

Model	Loss (α)	*NH*	*T*	*C*	*R*	# epochs	Time (s)
GT		0.929	0.990	0.976	0.277		
2K	Huber (1.0)	0.706	0.839	0.956	0.445	34	5.94
	Huber (5.0)	0.687	0.827	0.953	0.447	16	3.99
	Huber (10.0)	0.704	0.839	0.957	0.431	45	7.53
	Huber (20.0)	0.692	0.835	0.956	0.442	32	5.88
	Huber (30.0)	0.695	0.836	0.956	0.433	30	5.98
	logcosh	0.704	0.839	0.957	0.434	33	6.37
	MAE	**0.742**	**0.866**	**0.962**	**0.423**	78	11.05
	MSE	0.704	0.842	0.957	0.442	40	6.86
5K	Huber (1.0)	0.762	0.883	0.964	0.420	50	14.50
	Huber (5.0)	0.745	0.871	0.963	0.426	26	8.34
	Huber (10.0)	0.769	0.886	**0.965**	**0.416**	69	19.79
	Huber (20.0)	0.763	0.884	**0.965**	0.420	62	18.18
	Huber (30.0)	0.768	0.883	**0.965**	0.420	55	16.16
	logcosh	0.768	0.883	**0.965**	0.425	54	16.03
	MAE	**0.781**	**0.893**	**0.965**	0.418	57	16.56
	MSE	0.753	0.874	0.963	0.428	30	9.67
10K	Huber (1.0)	0.831	0.898	0.968	0.338	38	19.56
	Huber (5.0)	0.833	0.902	0.968	0.342	40	20.64
	Huber (10.0)	0.837	0.906	**0.969**	0.344	52	26.98
	Huber (20.0)	0.831	0.900	0.968	0.344	38	19.97
	Huber (30.0)	0.831	0.902	0.968	0.348	36	19.55
	logcosh	0.818	0.893	0.967	0.347	25	14.00
	MAE	**0.848**	**0.912**	0.968	**0.333**	58	29.55
	MSE	0.839	0.906	0.968	0.339	65	32.42
20K	Huber (1.0)	0.856	0.907	0.967	0.353	20	19.57
	Huber (5.0)	0.881	0.918	0.967	0.344	44	41.69
	Huber (10.0)	0.882	0.921	**0.968**	0.344	36	34.48
	Huber (20.0)	0.881	0.920	0.967	0.342	45	43.96
	Huber (30.0)	0.877	0.915	0.967	0.341	29	28.71
	logcosh	0.884	0.919	0.967	**0.335**	35	35.46
	MAE	**0.887**	**0.927**	0.966	0.339	47	44.55
	MSE	0.871	0.914	0.967	0.341	23	21.68

Table 7: Effect of **data augmentation**. Rows show metrics for t-SNE (*GT* row)) *vs* NN projections (other rows). Right two columns in each table show training effort (epochs and time). Bold shows values closest to *GT*.

a) **Noise after** strategy

Model	Noise σ	*NH*	*T*	*C*	*R*	# epochs	Time (s)
GT		0.929	0.990	0.976	0.277		
2K	0	0.717	0.846	0.958	0.448	31	8.84
	0.001	0.726	0.852	**0.960**	**0.430**	37	10.57
	0.01	**0.729**	**0.856**	**0.960**	0.433	54	14.52
5K	0	**0.783**	0.892	**0.966**	**0.401**	43	23.28
	0.001	0.780	**0.895**	**0.966**	0.408	52	29.44
	0.01	**0.783**	0.892	**0.966**	**0.401**	47	26.84
10K	0	**0.849**	0.909	**0.968**	0.339	44	44.06
	0.001	0.844	0.909	**0.968**	0.337	36	37.76
	0.01	0.848	**0.910**	**0.968**	**0.333**	59	60.31
20K	0	0.887	0.924	0.966	0.340	55	105.87
	0.001	**0.888**	0.924	**0.967**	**0.336**	46	88.09
	0.01	0.885	**0.925**	**0.967**	0.339	51	97.06

b) **Noise before** strategy

NH	*T*	*C*	*R*	# epochs	Time (s)
0.929	0.990	0.976	0.277		
0.712	**0.842**	0.957	0.446	23	7.17
0.679	**0.842**	**0.959**	0.422	33	9.57
0.682	0.833	0.956	**0.421**	20	6.86
0.785	**0.894**	0.966	0.401	62	33.34
0.793	0.884	0.966	**0.364**	31	17.91
0.802	0.888	**0.967**	0.366	49	28.68
0.849	**0.908**	**0.968**	0.336	36	35.61
0.798	0.901	0.966	0.304	37	39.58
0.802	0.904	0.966	**0.302**	53	55.58
0.888	**0.925**	**0.967**	**0.337**	40	76.08
0.865	0.920	**0.967**	0.385	42	81.55
0.869	0.920	**0.967**	0.392	41	80.52

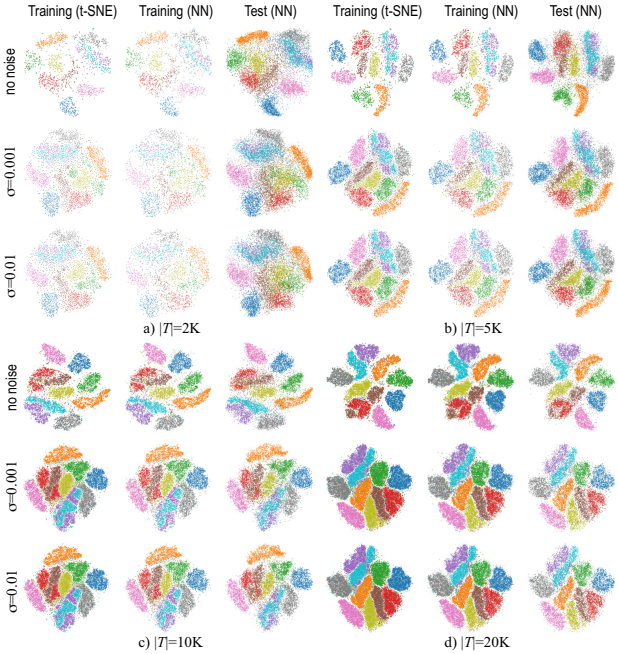

Figure 7: **Noise before** data augmentation: Effect of noise strength $\sigma \in \{0, 0.001, 0.01\}$. Compare the ground truth (training-set, projected by t-SNE) with the NN results on the training-set, respectively test-set.

achieves consistently the best quality metrics for almost all the tested cases, as compared to using the other loss functions. Separately, we see in Table 6 that the training effort for MAE is higher than when using the other loss functions. However, as the number of samples increases, the training-effort difference decreases, which is important, as it tells us that, for realistic (larger training-sets) cases, using MAE is not really costing more than using other loss functions. Given the quality increase, we conclude that MAE is the best loss function.

4.5 Network Architecture

Finally, we study the effect of using different NN architectures. Figure 9 shows that the architecture

Table 8: Effect of different **NN Architectures**. Rows show metrics for t-SNE (*GT* row) *vs* NN projections using different training-set sizes. Bold shows values closest to *GT*.

Model	NN Arch	*NH*	*T*	*C*	*R*	# epochs	Time (s)
GT		0.929	0.990	0.976	0.277	0	0
2K	small st	0.680	0.827	0.951	0.437	30	5.11
	small bt	0.670	0.819	0.950	0.453	18	3.85
	small wd	0.672	0.820	0.949	0.463	17	3.82
	medium st	0.683	0.827	0.952	0.441	17	3.83
	medium bt	0.690	0.833	0.955	0.456	25	4.96
	medium wd	0.702	0.838	0.956	0.438	44	7.17
	large st	0.692	0.835	0.956	0.447	19	4.66
	large bt	**0.720**	**0.852**	**0.961**	**0.430**	50	8.95
	large wd	0.713	0.847	0.959	0.434	45	8.30
5K	small st	0.744	0.875	0.962	0.414	66	18.31
	small bt	0.719	0.855	0.958	0.423	17	5.78
	small wd	0.726	0.864	0.959	0.424	40	12.21
	medium st	**0.761**	0.879	0.963	0.418	42	12.67
	medium bt	0.742	0.872	0.962	0.426	33	10.54
	medium wd	0.740	0.873	0.963	0.419	40	12.53
	large st	0.752	0.874	**0.964**	**0.408**	29	10.95
	large bt	**0.761**	**0.880**	**0.964**	0.420	34	12.02
	large wd	0.755	0.878	**0.964**	0.423	38	13.87
10K	small st	0.818	0.893	0.966	0.338	43	21.02
	small bt	0.820	0.893	0.966	0.330	54	27.35
	small wd	0.794	0.879	0.963	0.330	28	15.35
	medium st	0.828	0.900	0.968	0.343	45	22.74
	medium bt	0.820	0.895	0.967	0.343	31	16.68
	medium wd	0.825	0.899	0.967	**0.338**	49	25.74
	large st	0.831	0.902	0.968	**0.338**	32	20.34
	large bt	**0.836**	**0.905**	**0.969**	0.341	36	21.97
	large wd	0.830	0.900	0.968	**0.338**	30	19.31
20K	small st	0.865	0.910	0.965	**0.335**	30	30.81
	small bt	0.838	0.891	0.965	0.353	16	15.74
	small wd	0.865	0.910	0.965	0.345	37	34.66
	medium st	0.882	0.922	**0.967**	0.339	45	41.97
	medium bt	0.882	0.921	**0.967**	0.340	45	41.35
	medium wd	0.874	0.917	**0.967**	0.346	34	32.92
	large st	0.886	0.924	**0.967**	0.340	45	50.74
	large bt	**0.890**	**0.925**	**0.967**	0.342	37	42.48
	large wd	0.878	0.917	**0.967**	0.345	29	33.03

Large - bottleneck produces visual clusters that are slightly sharper than the ones created by the other architectures studied. This is confirmed by the quality metrics in Table 8: We see that *Large - bottleneck* has a *NH* about 0.04 higher for all training-set sizes. Also, while this architecture is larger than the others, its training effort is quite similar to that of the other architectures.

5 DISCUSSION

We next summarize the obtained insights, as follows.

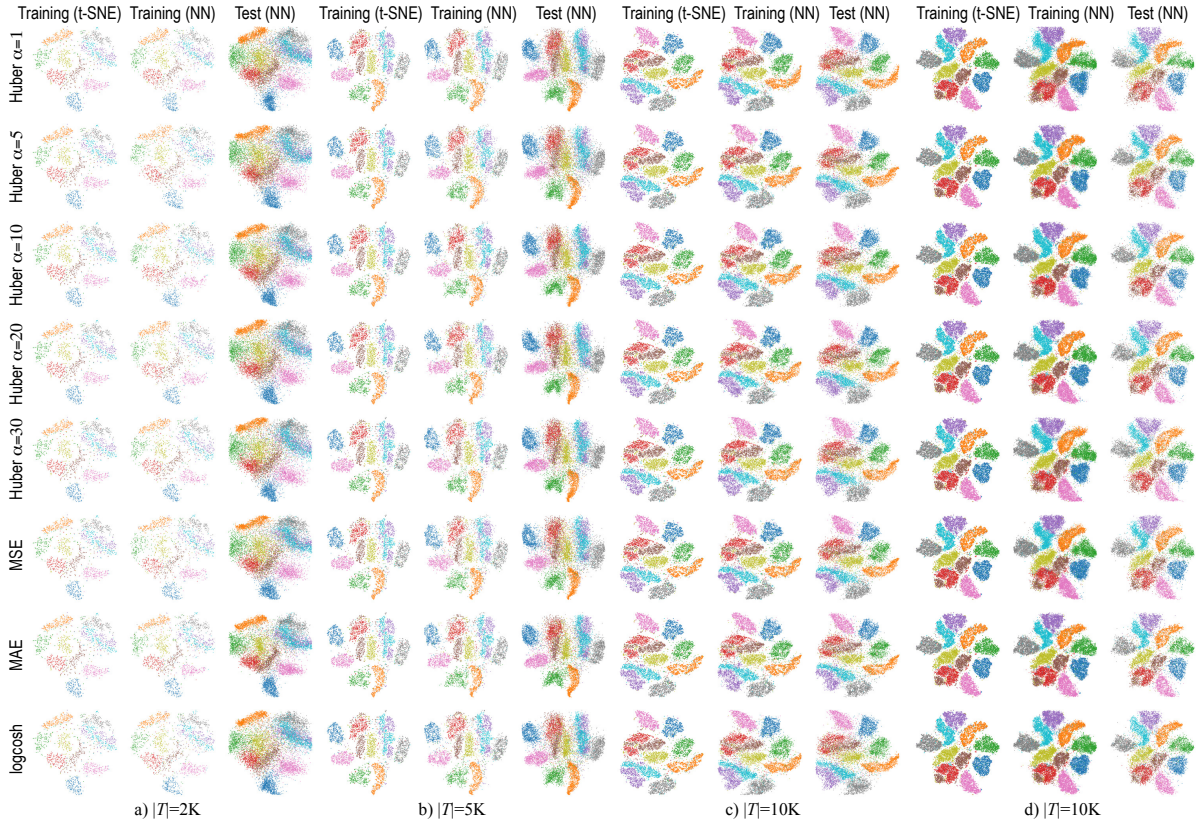

Figure 8: **Loss:** Effect of different loss functions. Compare the ground truth (training-set, projected by t-SNE) with the NN results on the training-set, respectively test-set.

Optimal settings: Our experiments showed that the proposed NN projection attains optimal quality (and closest to the ground-truth t-SNE projection) with no regularization, ADAM optimizer, *Noise after* data augmentation, MAE loss function, and *Large - Bottleneck* architecture. The choice of σ (noise standard deviation for data augmentation) affects very little the measured quality, so one should not be concerned in practice by how to set this parameter.

Given the above optimal settings, with $\sigma = 0.01$, we did one last experiment to evaluate how they perform when *combined*. We ran both the original *Std* architecture and the *Large - Bottleneck*, both using the optimal settings, to better assess the effect of the architecture change. In Table 9 we see that *Large - Bottleneck* performs better than *Std* on practically all metrics and for all training-set sizes. This improvement can be seen even when compared to the best results of each individual test, especially for smaller training-set sizes. Figure 10 shows this improvement in the form of less fuzziness and better separated clusters.

Quality: We have measured four well-known projection quality metrics: neighborhood hit, trustworthiness, continuity, and Shepard diagram correlation. Our experiments show that all these metrics are stable with respect to hyperparameter settings. More importantly, the optimal setting outlined above yields values which are very close to the ground-truth t-SNE values, and actually *closer* to ground-truth than the results presented in (Espadoto et al., 2019). As the training-set increases in size, the NN quality metrics *consistently* approach the ground-truth values – see Tables 3-8 for training-sets from 2K to 20K samples. The difference of the two is under 5% on average for training-sets of 20K points. We believe that this difference is a quite acceptable accuracy loss, given the simplicity, genericity, and high speed of the NN pro-

Table 9: Effect of using **optimal settings**. Metrics shown for t-SNE (*GT* row) *vs* NN projections using different training-set sizes. Bold shows values closest to *GT*.

Model	NN Arch	*NH*	*T*	*C*	*R*	# epochs	Time (s)
GT		0.929	0.990	0.976	0.277	0	0
2K	std	0.753	0.871	0.963	0.433	73	14.58
	large bt	**0.773**	**0.878**	**0.964**	**0.426**	82	18.44
5K	std	0.794	0.904	0.964	**0.411**	129	60.26
	large bt	**0.813**	**0.906**	**0.966**	**0.411**	70	37.19
10K	std	**0.850**	**0.916**	**0.967**	0.334	113	104.39
	large bt	**0.850**	0.913	0.966	**0.331**	108	112.53
20K	std	0.884	0.923	**0.964**	**0.335**	121	215.66
	large bt	**0.891**	**0.929**	**0.964**	**0.335**	101	205.07

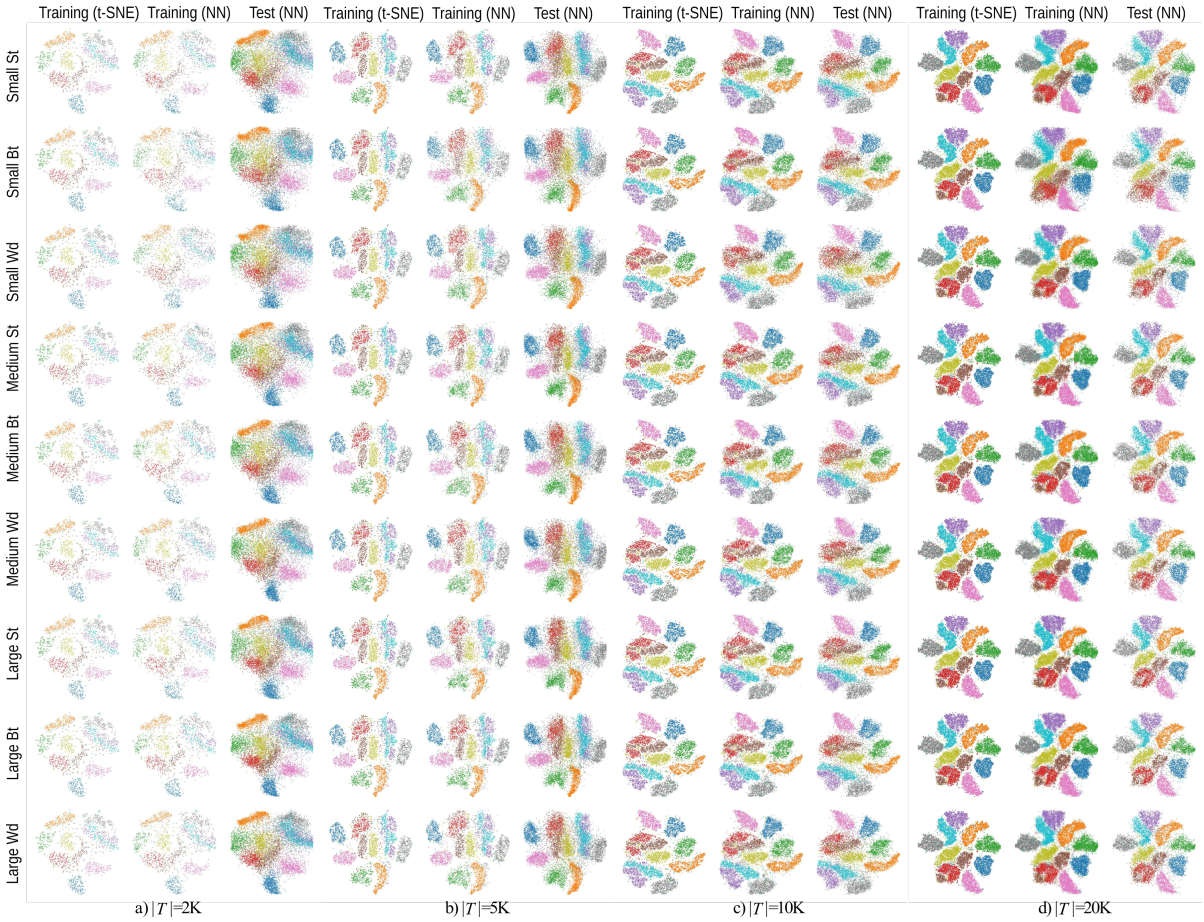

Figure 9: **NN Arch:** Effect of different NN Architectures. Compare the ground truth (training-set, projected by t-SNE) with the NN results on the training-set, respectively test-set.

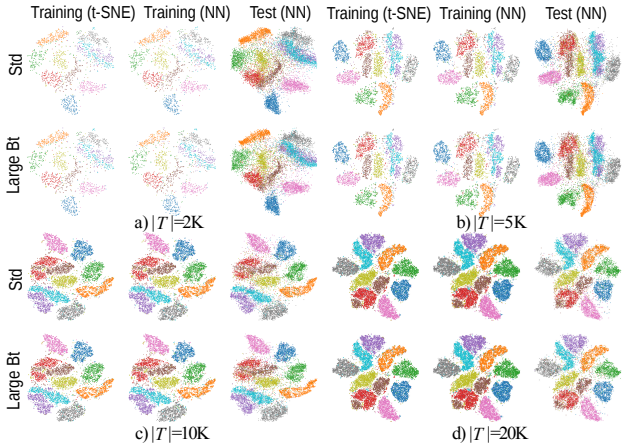

Figure 10: **Optimal Settings:** Effect of using optimal settings for *Std* and *Large - Bottleneck* NN architectures. Compare the ground truth (training-set, projected by t-SNE) with the NN results on the training-set, respectively test-set.

jection (all these aspects having been discussed in detail in (Espadoto et al., 2019)).

Visual examination of the NN projections shows that these exhibit a discernible amount of diffusion as compared to the ground-truth t-SNE projections. While diffusion clearly *decreases* with training-set size, it is still present even for the optimal parameter settings and 20K training samples – compare *e.g.* the inference on unseen data in Figure 7(d, test (NN)) with Figure 7(d, training, t-SNE).

Stability: An important result of our experiments is that the NN projection method is stable with respect to training-set sizes, hyperparameter settings, noise and loss functions. Indeed, Figures 2-9 show, regardless from the already discussed diffusion effect, practically the same *shape* and relative *positions* of the data clusters in the test projections (NN method run on unseen data) and the ground-truth t-SNE projections, for all tested configurations. The stability of the NN projection with respect to training data, parameter settings, and noise is in *stark contrast* with the instability of the ground-truth t-SNE projection with respect to *all* these three factors, and is of important practical added-value in

many applications (Wattenberg, 2016).

Improving projections: Following our analysis, the only noticeable drawback we see for the NN projections is the already discussed diffusion. Indeed, the main advantage of t-SNE praised by basically all its users is its ability to strongly separate similar-value sample clusters. Our experiments show that the NN projection can reach similar, though not fully identical, separation levels. Two open questions arise here: (1) How can we adapt the NN approach to learn such a strong separation? Our experiments show that hyperparameter settings, including regularization, data augmentation, optimizer, loss function and network architecture cannot fully eliminate diffusion, although by using MAE as loss function, quality metrics increased in value. The main open dimension to study is using non-standard *loss* functions than those used; (2) Can we design quality metrics able to better capture diffusion? If so, such metrics could be used to next design suitable loss functions to minimize this undesired effect. Both these issues are open to future research.

6 CONCLUSION

We presented an in-depth study aimed at assessing the quality and stability of dimensionality reduction (DR) using supervised deep learning. For this, we explored the design space of a recent deep learning method in this class (Espadoto et al., 2019) in six orthogonal directions: training-set size, network architecture, regularization, optimization, data augmentation, and loss functions. These are the main design degrees-of-freedom present when creating any deep learning architecture. We sampled each direction using several settings (method types and parameter values) and compared the resulting projections with the ground-truth (t-SNE method) quantitatively, using four quality metrics, and also qualitatively by visual inspection.

Our results deliver an optimal hyperparameter setting for which the deep-learned projections can approach very closely the quality of the t-SNE ground truth. Separately, we showed that the deep learning projection method is stable with respect to all parameter settings, training-set size, and noise added to the input data. These results complement recent evaluations (Espadoto et al., 2019) to argue strongly that supervised deep learning is a practical, robust, simple-to-set-up, and high-quality alternative to t-SNE for dimensionality reduction in data visualization. More broadly, this study is, to our knowledge, the only work that presents in detail how hyperparameter spaces of a projection method can be explored to find optimal settings and evidence for the projection method stability. We believe that our methodology can be directly used to reach the same goals (optimal settings and proof of stability) for any projection technique under study, whether using deep learning or not.

We plan to extend these results in several directions. First, we aim to explore non-standard loss functions to reduce the small, but visible, amount of diffusion present in the deep learned projections. Secondly, we aim to extend our approach to project time-dependent data in a stable and out-of-sample manner, which is a long-standing, but not yet reached, goal for high-dimensional data visualization.

ACKNOWLEDGMENTS

This study was financed in part by FAPESP (2014/12236-1, 2015/22308-2 and 2017/25835-9), CNPq (303808/2018-7) and the Coordenação de Aperfeiçoamento de Pessoal de Nível Superior - Brasil (CAPES) - Finance Code 001.

REFERENCES

Espadoto, M., Hirata, N., and Telea, A. (2019). Deep learning multidimensional projections. *arXiv:1902.07958 [cs.CG]*.

Feurer, M. and Hutter, F. (2019). Hyperparameter optimization. In *Automated Machine Learning*. Springer.

Hinton, G. E. and Salakhutdinov, R. R. (2006). Reducing the dimensionality of data with neural networks. *Science*, 313(5786):504–507.

Ilievski, I., Akhtar, T., Feng, J., and Shoemaker, C. (2017). Efficient hyperparameter optimization of deep learning algorithms using deterministic RBF surrogates. In *Proc. AAAI*.

Joia, P., Coimbra, D., Cuminato, J. A., Paulovich, F. V., and Nonato, L. G. (2011). Local affine multidimensional projection. *IEEE TVCG*, 17(12):2563–2571.

Jolliffe, I. T. (1986). Principal component analysis and factor analysis. In *Principal Component Analysis*, pages 115–128. Springer.

Kehrer, J. and Hauser, H. (2013). Visualization and visual analysis of multifaceted scientific data: A survey. *IEEE TVCG*, 19(3):495–513.

Kingma, D. and Ba, J. (2014). Adam: A method for stochastic optimization. *arXiv:1412.6980*.

Krogh, A. and Hertz, J. A. (1992). A simple weight decay can improve generalization. In *NIPS*, pages 950–957.

LeCun, Y., Cortes, C., and Burges, C. (2010). MNIST handwritten digit database. *AT&T Labs http://yann.lecun.com/exdb/mnist*, 2.

Liu, S., Maljovec, D., Wang, B., Bremer, P.-T., and Pascucci, V. (2015). Visualizing high-dimensional

data: Advances in the past decade. *IEEE TVCG*, 23(3):1249–1268.

Martins, R., Minghim, R., and Telea, A. C. (2015). Explaining neighborhood preservation for multidimensional projections. In *Proc. CGVC*, pages 121–128. Eurographics.

McInnes, L. and Healy, J. (2018). UMAP: Uniform manifold approximation and projection for dimension reduction. *arXiv:1802.03426*.

Nonato, L. and Aupetit, M. (2018). Multidimensional projection for visual analytics: Linking techniques with distortions, tasks, and layout enrichment. *IEEE TVCG*.

Park, M. Y. and Hastie, T. (2007). L1-regularization path algorithm for generalized linear models. *J Royal Stat Soc: Series B*, 69(4):659–677.

Paulovich, F. V., Nonato, L. G., Minghim, R., and Levkowitz, H. (2008). Least square projection: A fast high-precision multidimensional projection technique and its application to document mapping. *IEEE TVCG*, 14(3):564–575.

Peason, K. (1901). On lines and planes of closest fit to systems of point in space. *Philosophical Magazine*, 2(11):559–572.

Qian, N. (1999). On the momentum term in gradient descent learning algorithms. *Neural networks*, 12(1):145–151.

Rauber, P., Falcão, A. X., and Telea, A. (2016). Visualizing time-dependent data using dynamic t-SNE. In *Proc. EuroVis: Short Papers*, pages 73–77.

Roweis, S. T. and Saul, L. K. (2000). Nonlinear dimensionality reduction by locally linear embedding. *Science*, 290(5500):2323–2326.

Srebro, N. and Shraibman, A. (2005). Rank, trace-norm and max-norm. In *Intl. Conf. on Computational Learning Theory*, pages 545–560. Springer.

Tenenbaum, J. B., De Silva, V., and Langford, J. C. (2000). A global geometric framework for nonlinear dimensionality reduction. *Science*, 290(5500):2319–2323.

Torgerson, W. (1958). *Theory and Methods of Scaling*. Wiley.

van der Maaten, L. and Hinton, G. E. (2008). Visualizing data using t-SNE. *JMLR*, 9:2579–2605.

van der Maaten, L. and Postma, E. (2009). Dimensionality reduction: A comparative review. Technical report, Tilburg Univ., Netherlands. TiCC 2009-005.

Venna, J. and Kaski, S. (2006). Visualizing gene interaction graphs with local multidimensional scaling. In *Proc. ESANN*, pages 557–562.

Wattenberg, M. (2016). How to use t-SNE effectively. `https://distill.pub/2016/misread-tsne`.

Wilson, A., Roelofs, R., Stern, M., Srebro, N., and Recht, B. (2017). The marginal value of adaptive gradient methods in machine learning. In *NIPS*, pages 4148–4158.

Yao, Y., Rosasco, L., and Caponnetto, A. (2007). On early stopping in gradient descent learning. *Constructive Approximation*, 26(2):289–315.